THE JOURNAL OF PHYSICAL CHEMISTRY C

Article

pubs.acs.org/JPCC

Mechanisms of Zinc Oxide Nanocrystalline Thin Film Formation by Thermal Degradation of Metal-Loaded Hydrogels

Ilenia G. Tredici,[†] Alessandro Resmini,[†] Sonia Pin,[†,‡] Paolo Ghigna,[†] Tommaso Rovetta,[§] Maddalena Patrini,[∥] Nicola Rotiroti,[⊥] Monica Dapiaggi,[⊥] and Umberto Anselmi-Tamburini*[,†]

[†]Department of Chemistry, University of Pavia, Viale Taramelli 12, I-27100 Pavia, Italy

[‡]General Energy Research (ENE), Laboratory for Bioenergy and Catalysis, Paul Scherrer Institut, 5232 Villigen, Switzerland

[§]Centro Interdipartimentale di Studi e Ricerche per la Conservazione del Patrimonio Culturale (CISRiC), Laboratorio Arvedi, University of Pavia, via Ferrata 1, I-27100 Pavia, Italy

[∥]Department of Physics, University of Pavia, Via Bassi 6, I-27100 Pavia, Italy

[⊥]Department of Earth Science, University of Milan, Via Botticelli 23, I-20133 Milano, Italy

Supporting Information

ABSTRACT: Thermal degradation of metal-loaded hydrogel films is a powerful tool to synthesize high-quality metal oxide thin films with nanometric grain size, but the formation mechanism is still poorly known. We exploited fluorescence X-ray absorption fine structure as a short-range probe to investigate the first stages of nucleation and the following development of ZnO nanoparticles in Zn-loaded hydrogels, annealed for 20 min at temperatures between 150 and 500 °C. The experimental results evidenced that the first nuclei of ZnO begin to form at 300 °C, whereas at 350 °C the ZnO nanoparticles are already well crystallized. By coupling the results with those obtained by thermal analysis, profilometry, HR-TEM, diffraction and μ-FTIR, a formation mechanism was suggested. The optical and electrical properties of the samples confirm that the polymer forms an insulating shell around the nanoparticles up to 450 °C: the intimate hybridization promotes stress relaxation during the annealing, yielding crack-free metal oxide films. Prolongation of the annealing time allowed the removal of the organic shell at 350 °C, yielding fully conductive, transparent ZnO films with particle size reduced to 7 nm.

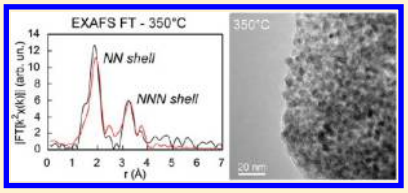

1. INTRODUCTION

In the past few years, ZnO has received much attention due to its unique and outstanding combination of physicochemical properties. Because of its wide direct band gap (E_g ~ 3.3 eV at 300 K) and its large exciton binding energy (~60 meV), it is actively investigated for optoelectronic applications, while its high optical transparency and chemical stability under light exposure make it attractive as a transparent electrode in flat-panel displays,[1] solar cells, and thin-film transistors.[2,3] Other recent reports account for ZnO application in lasing,[1] spintronics,[1] microelectromechanical systems (MEMS),[4,5] and gas sensing.[6,7]

Deposition of thin films of ZnO and of other metal oxides represents a key step in most of these technological applications; RF sputtering, molecular beam epitaxy, chemical vapor deposition, and metal−organic vapor phase epitaxy have proved to be effective in the deposition of high quality thin films of ZnO and other metal oxides.[8−11] However, all these techniques involve the use of costly and complex experimental apparatus and, in some cases, of toxic chemical precursors. Furthermore, none of these methods allow a simple direct patterning of the produced film. Alternative low-cost approaches based on solution chemistry deposition methods have been recently proposed, although in most cases costly or toxic chemical precursors are still required, while patterning capabilities are generally poor.[12,13]

Recently, we introduced a novel solution method for the deposition of thin films of ceramic oxides, based on the use of metal-loaded hydrogels.[14−16] Hydrogels are able to incorporate large amounts of metal ions, soluble in simple solvents (such as water or simple alcohols), and can easily be deposited by spin- or dip-coating and photopolymerized, so they represent an ideal precursor for film deposition. Furthermore, hydrogels can effectively be patterned on a micro and submicro scale using soft lithographic techniques. A nanocrystalline metal oxide thin film can then be easily obtained through thermal degradation of the hydrogel. This method was effective in producing high quality patterned thin films of several different metal oxides,[14−16] avoiding some typical drawbacks presented by other solution deposition techniques, particularly those based on sol−gels, such as film cracking and low quality patterning.[16] Oxide thin films obtained by using the hydrogel method have a remarkable nanostructure, characterized by regular rounded nanograins, having, in the case of ZnO, a significant preferred orientation, a characteristic that made them an ideal seeding layer for the growth of patterned ZnO nanorods.[17]

A meaningful knowledge of the mechanism of formation of the ZnO nanocrystals during the thermal degradation of the

Received: August 9, 2013
Revised: October 22, 2013
Published: October 30, 2013

dx.doi.org/10.1021/jp407993q | J. Phys. Chem. C 2013, 117, 25108−25117

hydrogel is particularly interesting in view of an even better control of the nanostructure and of the application of the method to the synthesis of complex oxides, containing several different cations. The formation mechanisms of films of ZnO nanoparticles have been described previously, but mostly in the case of sol−gel or thermal degradation of simple salts.[18−20] Only few papers investigated the oxide formation mechanism in the case of polymer assisted deposition.[21,22] These studies generally suggest that the metal oxides particles start to form when the massive thermal decomposition of the polymers begins, at temperatures around 450−500 °C.[21,22] However, a detailed investigation of the mechanism, offering clear information on the nucleation and the subsequent development of oxide nanoparticles, is still lacking. This is due in part to the difficulties in detecting the early stages of the oxide nucleation,[21] mostly because some of the techniques used, such as Raman, X-ray diffraction (XRD), and thermal analysis, are not sensitive enough to detect the early stage of the process. Our previous investigations[14] have already shown, by means of grazing incidence diffraction (GID), that in the case of the thermal decomposition of metal-loaded hydrogels the first crystallization of ZnO nanoparticles begins at 450 °C, while full crystallization of the ZnO phase is observed only at temperatures as high as 500 °C. However, these results were affected by the low sensitivity of the technique, which cannot detect the formation of small, poorly crystallized nuclei.

In this paper we report a detailed investigation on the nucleation and subsequent growth of ZnO nanoparticles during the thermal degradation of cross-linked metal-loaded hydrogels, coupling fluorescence X-ray absorption fine structure (fluo-XAFS) measurements with thermal analysis, profilometry, high-resolution transmission electron microscopy (HR-TEM), X-ray and electron diffraction, μ-Fourier transform infrared (μ-FTIR) spectroscopy, and optical and electrical characterizations, all performed at different stages of the degradation process. On the basis of these results, a possible formation mechanism will be proposed.

2. EXPERIMENTAL DETAILS

All reactants and solvents were purchased from Sigma-Aldrich and used as received. The ZnO thin films were grown on glass substrates by spin-coating and photopolymerization of a hydrogel precursor loaded with $Zn(NO_3)_2$. The hydrogel was based on the copolymerization of two moieties: poly(ethylene glycol) dimethacrylate (PEG-DMA, M_n 550) and trimethylolpropane benzoate diacrylate. Further details about the precursor composition, spinning conditions, and photopolymerization can be found in the Supporting Information.

After preparation, the polymeric film was annealed in a furnace at various temperatures between 150 and 550 °C and maintained at that temperature for 20 min. After the heat treatment the films were characterized with fluorescence X-ray absorption fine structure (XAFS). The results were coupled with those obtained using thermal analysis, profilometry, grazing incidence diffraction (GID), high-resolution transmission electron microscopy (HR-TEM), selected area electron diffraction (SAED), and μ-Fourier transform infrared (μ-FTIR) spectroscopy. Optical and electrical characterization was performed using UV−vis absorption, photoluminescence (PL), and impedance spectroscopy. See Supporting Information for experimental details.

3. RESULTS

3.1. Microstructure and Film Thickness. Upon annealing at 500 °C, the Zn-loaded hydrogel produces a homogeneous thin film of nanocrystalline ZnO characterized by a grain size of 15−20 nm, when the precursor concentration is 0.30 M. The thickness of the film is of 120−150 nm, but it can be varied between 40 nm and 1 μm, changing the metal precursor concentration between 0.05 and 1 M and adjusting the spinning conditions.[14−16] The film has a uniform microstructure, characterized by well-sintered round nanoparticles, which were observed in the cross-section and top-view scanning electron micrographs of Figure 1. The film is crack-free and

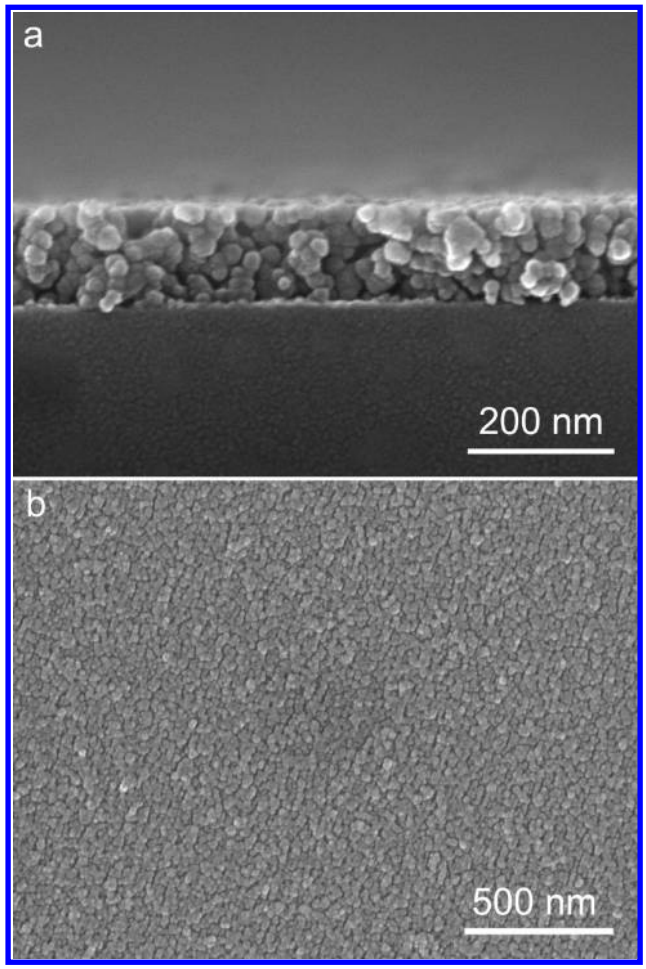

Figure 1. Scanning electron micrographs: (a) cross section of the ZnO film obtained after degradation of the hydrogel at 500 °C; (b) top view of the same film.

well adherent to the substrate, despite the huge volume contraction associated with the thermal degradation of the organic matrix, observed by profilometric analysis. Figure 2 shows the thickness of the film at different stages of thermal degradation: the final film thickness is indeed ∼2% of the starting value. Interestingly, the thickness seems to linearly decrease up to 400 °C, while the final value is reached only for $T \geq 400$ °C, suggesting that organic byproducts could still persist for lower temperatures.

3.2. Thermal Analysis. The main features associated with the thermal degradation of the hydrogel have already been discussed in a previous work[14] and will be only briefly summarized here (Figure 3). Upon heating, a first relevant

dx.doi.org/10.1021/jp407993q | J. Phys. Chem. C 2013, 117, 25108−25117

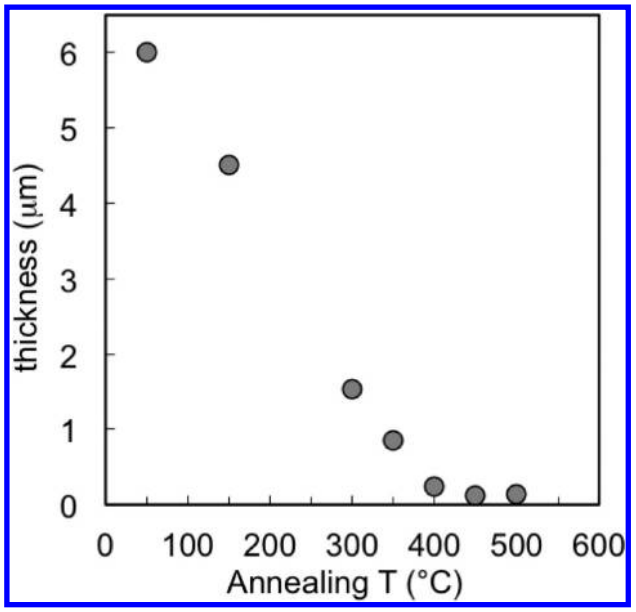

Figure 2. Profilometric analysis of the film thickness as a function of annealing temperature.

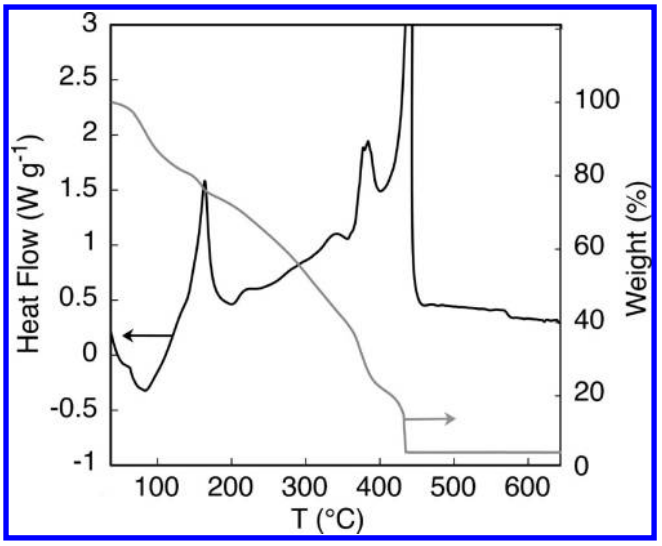

Figure 3. Thermal analysis of the degradation of the zinc-loaded hydrogel in pure oxygen; heating rate 5 °C min^{-1} (black line: heat flow; gray line: weight loss). Adapted from ref 14.

weight loss is observed at around 100 °C; this weight loss is associated with an endothermic event, which is probably due to the removal of the residual solvent. The exothermic peak at ~150 °C is attributed to a rearrangement of the PEG molecules because it was detected also when degradation is performed in nonoxidative atmosphere (nitrogen, not shown). Between 200 and 400 °C a fairly continuous weight loss is observed, probably associated with the gradual degradation of the organic matrix, which is concluded by two exothermic peaks at ~400 and ~450 °C. After the final exothermic event the weight of the sample reached its final value, corresponding to the sole ZnO product, confirming what suggested by profilometric measurements.

3.3. EXAFS Analysis. XANES spectra of the precursor films annealed at various temperatures are reported in Figure 4, together with the spectrum relative to pure ZnO (in powder form) as a reference. For the sake of clarity, all the spectra are

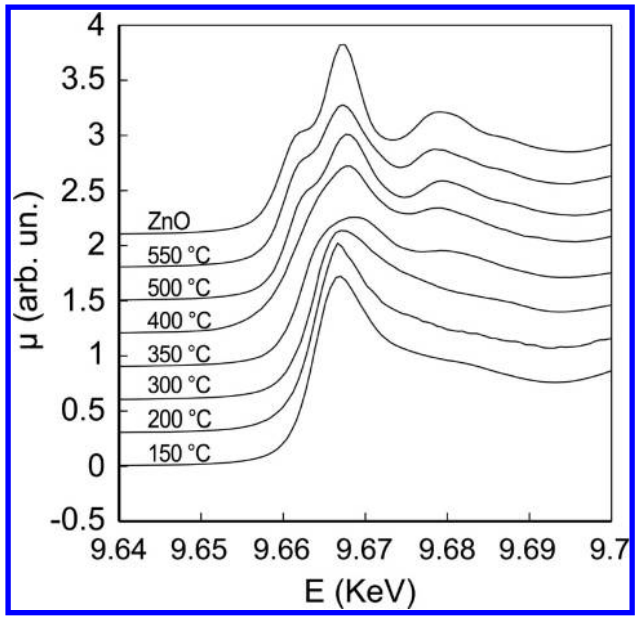

Figure 4. XANES spectra of the films after increasing annealing temperature compared to ZnO powder as a reference.

here displayed shifted along the *y*-axis. Upon increase in the annealing temperature the XANES manifold at the Zn−K edge undergoes a well-evident change from an almost structureless shape to a ZnO-like structure.[23−25] Since XANES spectroscopy can be used for fingerprinting crystallographic phases, this is a clear indication that the thermal treatments cause the polymeric precursor to yield a wurtzite-type ZnO phase. This process is apparently concluded after 550 °C. In samples annealed at lower temperatures, the structures in the XANES manifold are less evident, indicating a higher level of disorder. This can be interpreted in terms of degree of crystallinity: the lower the heating temperature, the lower the degree of crystallinity of the produced ZnO crystals. This smearing out of the XANES manifold is well apparent in the range $350 \leq T \leq 550$ °C. At lower temperatures, the XANES manifolds are fairly different in shape, the lack of characteristic features being indicative of Zn in an amorphous environment.

This interpretation is well supported by the EXAFS spectra shown in Figure 5 and by the EXAFS FT of Figure 6. The EXAFS FT can be assimilated to a radial distribution function (RDF) around the photoabsorber: the peaks in the EXAFS FT can be attributed to coordination shells, with the warnings that the apparent distances in the EXAFS FT differ from the effective distances in the actual compound due to the phase shifts of the photoelectron wave, while the amplitudes depend on the actual scattering functions of neighboring atoms. In any case, while the presence of a nearest-neighbor (NN) shell around 2 Å is well evident at all temperatures, the appearance of a next-nearest-neighbor (NNN) shell at ca. 3.2 Å is detected without doubts only for the film treated at $T \geq 350$ °C. The presence of a NNN shell in an EXAFS spectrum is typical of crystals; glassy and amorphous phases usually show just a NN shell. Thus, the EXAFS data fully confirm the interpretation of the XANES given above: crystals of ZnO start to form at $T = 350$ °C. For $T \geq 500$ °C, the presence of a further NNN coordination shell at ca. 4.5 Å suggests that crystallization is here almost complete.

More quantitative information was retrieved by the EXAFS data fitting. The fitting results are summarized in Table 1, while

dx.doi.org/10.1021/jp407993q | J. Phys. Chem. C 2013, 117, 25108−25117

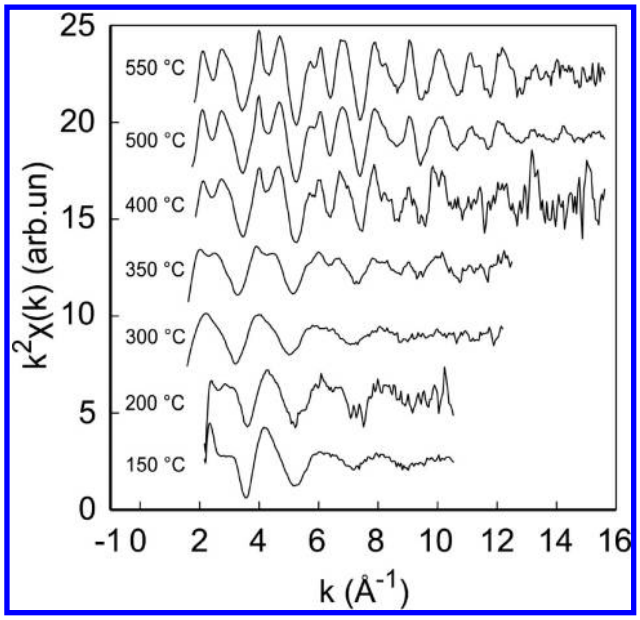

Figure 5. EXAFS spectra of the films after increasing annealing temperature.

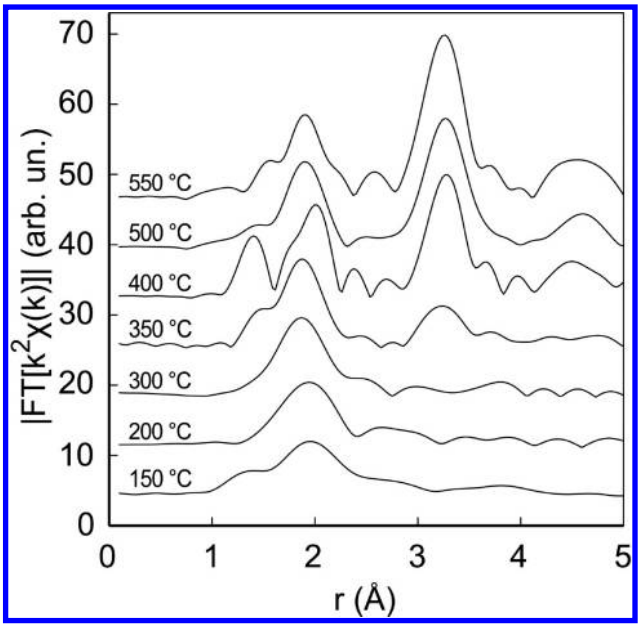

Figure 6. EXAFS FT of the films after increasing annealing temperature.

Figure 7 shows the best fit for samples annealed at 150, 350, and 500 °C (upper part: EXAFS spectra; lower part: FT; the fit results are plotted as red lines, while black lines are the experimental data). For the sample heated at 150 °C (Figure 7a), the best fit has been obtained by using a model in which 4 O atoms and 2 N atoms are located around the photoabsorber. This may be indicative of Zn coordinated by nitrate ions in a distorted tetrahedral environment.[26] It should be noted that EXAFS could not distinguish between N and C as neighbors of the photoabsorber, so this fit is also compatible with Zn surrounded by a polymeric matrix. Similar considerations apply also to the sample heated at 200 °C; the results of the fit are shown in Table 1 as well.

Table 1. EXAFS Fitting Results of the Samples Annealed at 150, 200, 300, 350, and 500 °C

shell	N	atom	r (Å)	σ^2 (Å^2)	r_0 (Å)
150 °C					
1	2	O	1.96(1)	$2(1) \times 10^{-3}$	
2	2	O	2.10(2)	$3(2) \times 10^{-3}$	
3	2	N	2.80(5)	$11(8) \times 10^{-3}$	
200 °C					
1	4	O	2.01(2)	$7(2) \times 10^{-3}$	
2	2	N	2.71(8)	$15(10) \times 10^{-3}$	
300 °C					
1	1	O	2.32(3)	$6(2) \times 10^{-3}$	1.796
2	3	O	2.061(9)	$6(2) \times 10^{-3}$	2.042
3	6	Zn	2.9(2)	$10(5) \times 10^{-2}$	3.2089
4	6	Zn	3.41(4)	$3(1) \times 10^{-2}$	3.2490
350 °C					
1	1	O	2.30(3)	$4(1) \times 10^{-3}$	1.796
2	3	O	2.027(9)	$4(1) \times 10^{-3}$	2.042
3	6	Zn	3.25(1)	$8(2) \times 10^{-3}$	3.2089
4	6	Zn	3.46(2)	$1.0(5) \times 10^{-2}$	3.2490
500 °C					
1	1	O	2.00(1)	$8(2) \times 10^{-3}$	1.796
2	3	O	2.00(1)	$8(2) \times 10^{-3}$	2.042
3	6	Zn	3.22(1)	$4(2) \times 10^{-3}$	3.2089
4	6	Zn	3.33(4)	$8(4) \times 10^{-3}$	3.2490

For T = 300 °C, EXAFS oscillations in a wider k range are detected. In this case, a wurtzite-type ZnO structure has been used for the fit, although the presence of a NNN coordination shell appears arguable. Best-fit results are shown in Table 1 along with the crystallographic parameters (r_0) for ZnO. For T = 350 °C, the presence of a NNN shell is detected without doubts. The fit is shown in Figure 7b, and the fitting results are summarized in Table 1.

At higher temperatures the EXAFS spectra are all compatible with a ZnO-like crystal structure. As an example in Figure 7c are shown the results for the sample annealed at 500 °C, while the optimized parameters for this sample are reported in Table 1.

All these observations suggest the formation of wurtzite-type ZnO nuclei in the polymeric matrix starting from temperatures of 300−350 °C. As the temperature is increased, the nuclei grow and the crystallization process is concluded for $T \geq 500$ °C.

3.4. GID, HR-TEM, and SAED. Previous GID measurements[14] showed some evidence of crystallization only in samples annealed at temperatures above 450 °C. A more accurate analysis, performed by increasing the counting time up to 450 s per step, evidenced the presence of a broad halo in the 2θ range corresponding to the position of the (100), (002), and (101) reflections for hexagonal ZnO, even in samples annealed at 400 °C (Figure 8). The presence of this halo is better evidenced when comparing the pattern with that relative to a sample annealed at 350 °C, which shows only a flat background. In contrast with our previous findings,[14] using such long acquisition time, the pattern relative to the sample annealed at 450 °C has three well-developed peaks, indicating some level of crystallization of the wurtzitic structure. The grain sizes, which could be measured only on samples obtained at 450 and 500 °C, were around 15 and 20 nm, respectively. In contrast with the EXAFS measurements no indication of the presence of ZnO small nuclei in samples annealed at 350 °C

dx.doi.org/10.1021/jp407993q | J. Phys. Chem. C 2013, 117, 25108−25117

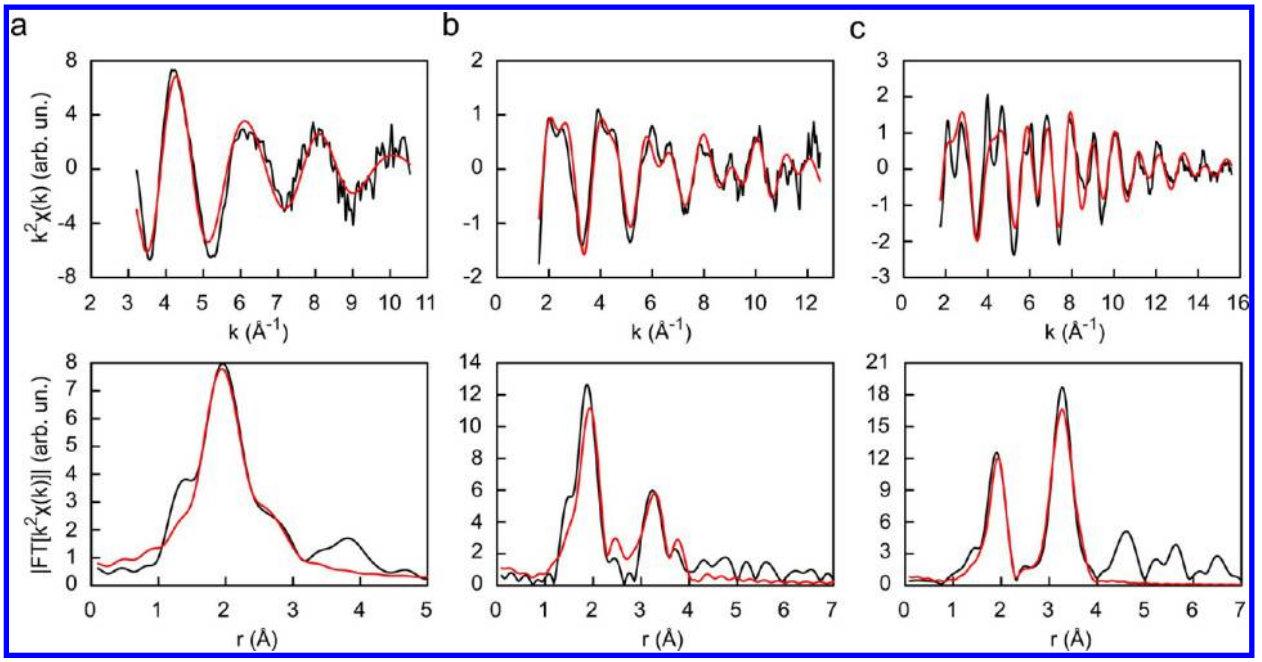

Figure 7. EXAFS data fitting. EXAFS spectrum (upper part) and FT (lower part) of the samples heated at 150 (a), 350 (b), and 500 °C (c). Red line: fit; black line: experimental. For fitting results see Table 1.

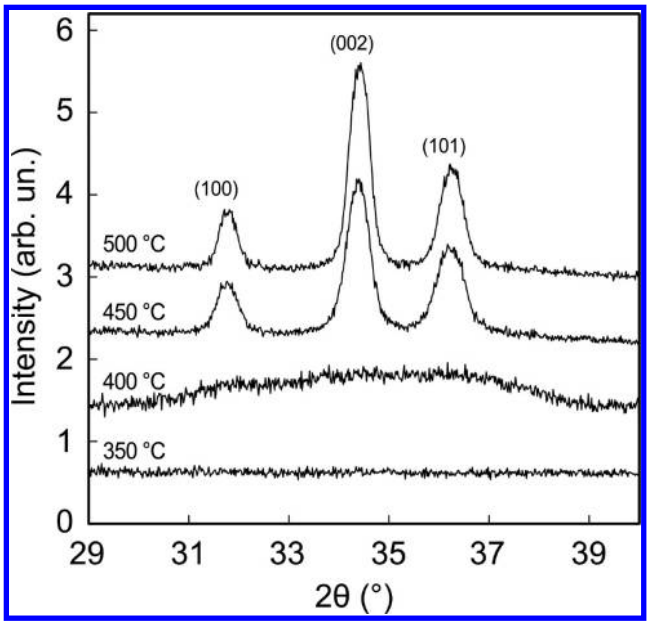

Figure 8. GID patterns of the samples degraded at 350, 400, 450, and 500 °C.

were obtained; the absence of diffraction effects for samples annealed at this temperature is probably due to the reduced grain size, too small to provide long-range order, necessary to give X-ray diffraction,[27] while short-range order around the photoabsorbers (Zinc atoms) can be revealed by EXAFS measurements.

To confirm these results, HR-TEM analysis has been performed on hydrogels annealed at 350 and 400 °C (Figure 9). Indeed, both samples have crystalline grains embedded in an amorphous matrix, as evidenced by both TEM bright field images and electron diffraction measurements. SAED patterns (Figures 9a and 9d) confirm the hexagonal ZnO structure for the nuclei present in both samples, although the sample annealed at the lowest temperature has a smaller amount of crystallites, as indicated by the lower intensity and definition of the diffraction rings. High-resolution images reveal spherical shaped grains with an average grain size of around 3 nm for the sample annealed at 350 °C and 6 nm for the sample annealed at 400 °C. The SAED pattern acquired on the sample annealed at 400 °C shows the signals corresponding to the (100), (002), and (101) reflections merged in a single halo, a behavior similar to that observed in the same range in the GID patterns.

3.5. Optical Properties: UV−vis and PL Spectroscopy.

As already reported in our previous work,[14] films obtained after complete thermal degradation at 500 °C are characterized by high optical transparency. In Figure 10 is shown the evolution of the UV−vis transmittance of the films during the thermal degradation of the hydrogel, as measured on samples annealed at temperatures ranging between 150 and 500 °C. The as-deposited films of metal-loaded hydrogel have the optical properties of a transparent polymer with a slight yellow coloration. Upon annealing, the films tend to discolor toward a brownish-yellow hue, resulting in a lower transmittance at all wavelengths, particularly for the samples annealed between 250 and 350 °C. At 400 °C the transmittance starts to increase again and an absorption edge around 390 nm starts to appear. At 450 °C the polymer combustion is complete, and the samples are highly transparent. The typical sharp absorption edge around 385 nm is observed in the last two samples, confirming the presence of a band gap at about 3.25 eV, close to the value expected for pure ZnO (3.3 eV[1]). (The data were plotted as recorded and not rescaled as a function of the film thickness because the aim was to evaluate the appearance of the ZnO absorption edge after annealing.)

The PL spectra reported in Figure 11 show only one broad band located between 360 and 700 nm, probably associated with the organic matrix of the precursor, in samples annealed at temperatures below 400 °C. At 400 °C this band disappears, while a band typical of ZnO,[1] located between 340 and 420 nm, begins to appear. This band increases in intensity in samples

dx.doi.org/10.1021/jp407993q | J. Phys. Chem. C 2013, 117, 25108−25117

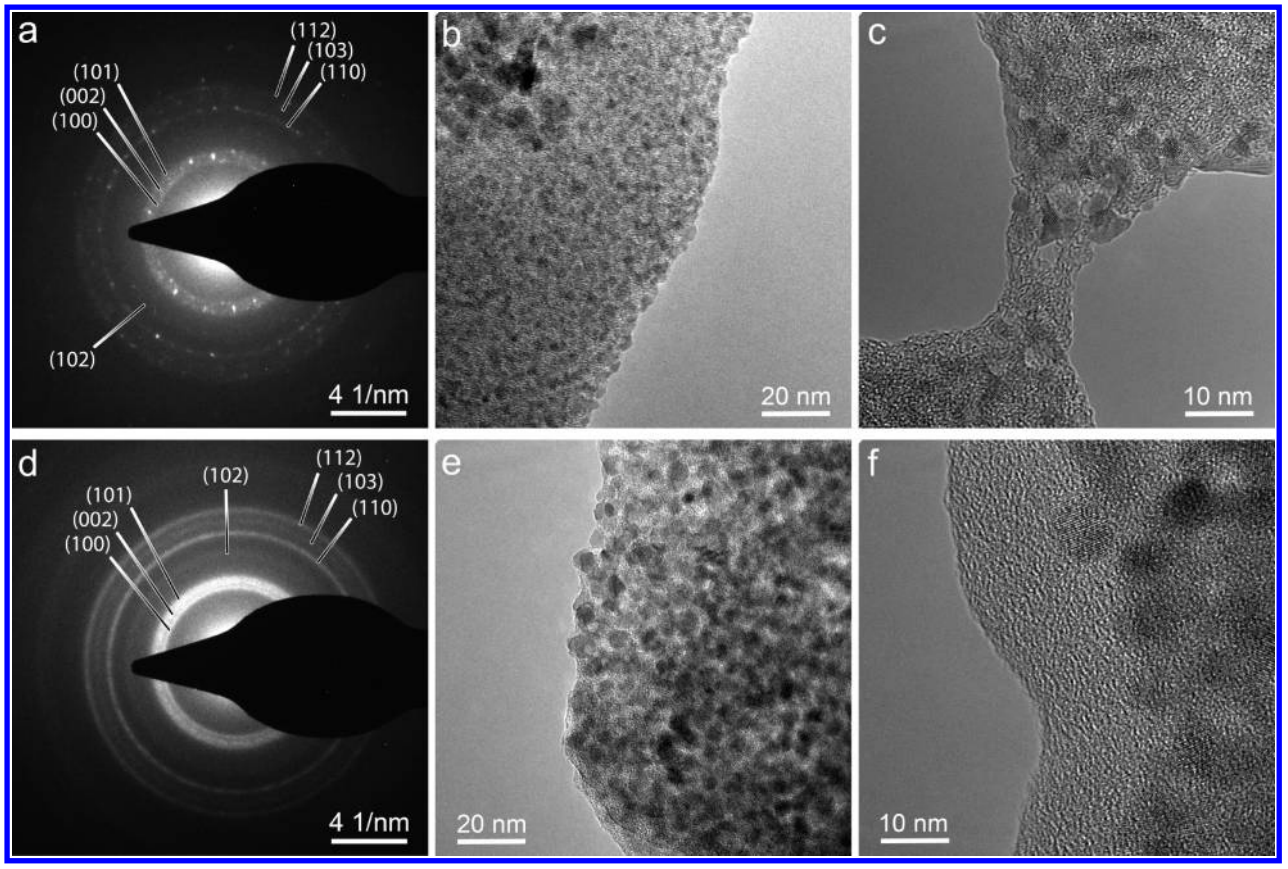

Figure 9. Transmission electron micrographs of the samples degraded at 350 °C (a–c) and 400 °C (d–f): (a, d) SAED (selected area electron diffraction); (b, e, c, f) HR-TEM images.

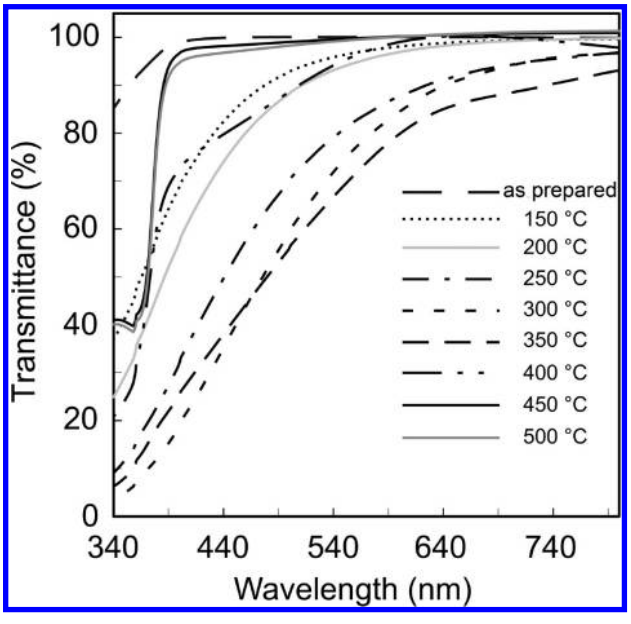

Figure 10. Optical characterization. UV–vis transmittance spectra of the films for increasing annealing temperature.

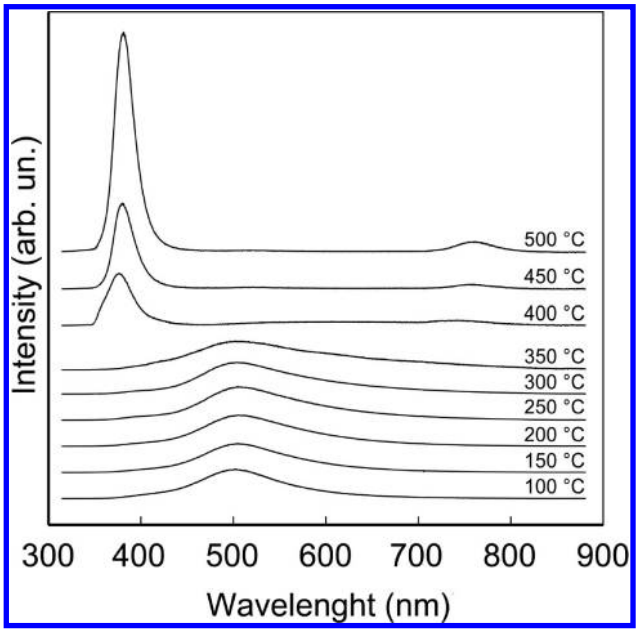

Figure 11. PL spectra of the films for increasing annealing temperature. The signals intensity for the samples annealed at 450 and 500 °C were reduced to 40% of the original value.

annealed at higher temperatures, together with the related small emission signal at twice its wavelength. From the first signal a band gap between 3.31 and 3.28 eV was calculated, in agreement with the results obtained from UV–vis spectra.

3.6. Electrical Properties: Impedance Spectroscopy. Impedance measurements were performed on samples annealed between 150 and 500 °C. A significant electrical conductivity is expected only in samples characterized by the presence of percolating, interconnected, ZnO particles, so the electrical conductivity represents a sensitive probe for the presence of organic material surrounding the grains of the

dx.doi.org/10.1021/jp407993q | J. Phys. Chem. C 2013, 117, 25108–25117

oxide. Since it was preferable to perform the measurements at low temperatures (to avoid further thermal degradation), the impedance measurements have been performed at room temperature, but under UV exposure (one lamp, 15 W, λ_{max} = 310 nm, placed at 5 cm from the sample) to enhance the electronic conductivity.[28]

A measurable specific conductivity of 5.9×10^{-5} Ω^{-1} cm^{-1} was obtained only for the samples annealed at 450 and 500 °C. The sample annealed at 400 °C was characterized by a resistivity far beyond the limit of detection of the instrument, even under UV exposure. These results suggest that the ZnO nanoparticles are still capped by a polymeric matrix at temperatures up to 400 °C, and only for $T \geq 450$ °C percolating path between the ZnO grains starts to develop.

3.7. μ-FTIR Analysis. Figure 12 shows the evolution of μ-FTIR spectra for Zn-loaded hydrogels films annealed at

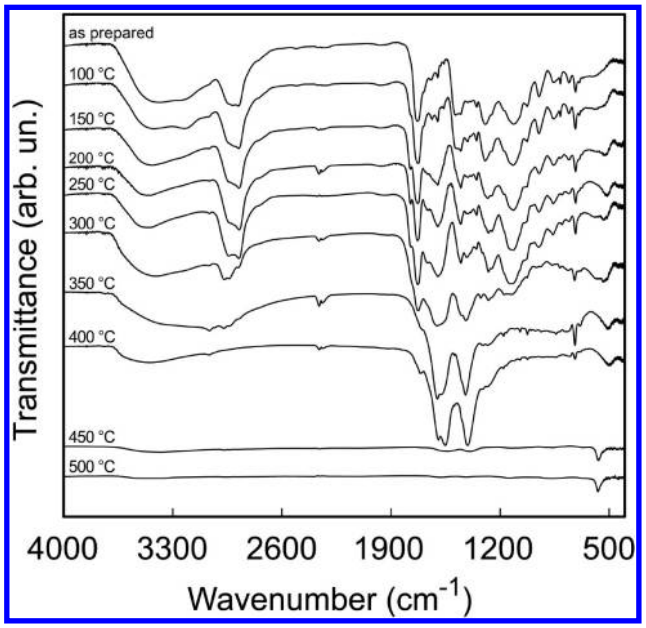

Figure 12. μ-FTIR spectra of the films for increasing annealing temperature.

different temperatures. The spectrum of the as-prepared films is characterized by the presence of several well-defined absorption bands associated with the vibrational modes of the main functional groups of the polymer. These were assigned as follows: the bands at 1100 and 1730 cm^{-1} are relative to the stretching modes of the C−O ether groups and C═O esteric groups, respectively; the bands at 2962−2850 cm^{-1} are relative to the stretching of CH_3 and CH_2 aliphatic groups; at 1450 cm^{-1} is present the bending mode of CH_2; the broad band at 3400 cm^{-1} is relative to the stretching mode of the O−H group deriving either from the hydroxy-Zn intermediates or from adsorbed water. At ∼1400 and ∼1600 cm^{-1} are present the absorption bands of the carboxylate groups, probably ascribable to symmetric and asymmetric stretching of C═O, respectively.[29,30]

The evolution of the intensity of these bands during the thermal degradation is reported in Figure 13. (The points corresponding to 50 °C refer to the as-prepared film. The data were not rescaled as a function of the film thickness because we wanted to probe the absolute amount of the materials present in the film and not their relative concentration.) Most of these

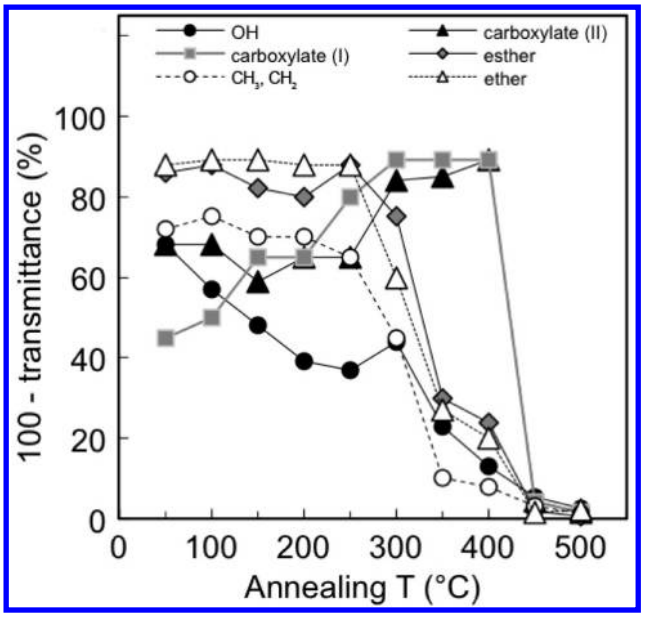

Figure 13. Intensity of the main μ-FTIR signals for increasing annealing temperature. The points corresponding to 50 °C refer to the as-prepared film. Black circles: OH at 3400 cm^{-1}; gray squares: carboxylate at ∼1600 cm^{-1}; open circles: aliphatic CH_3 and CH_2 at ∼2900 cm^{-1}; black triangles: carboxylates at ∼1400 cm^{-1}; gray diamonds: C═O ester at 1730 cm^{-1}; open triangles: C−O PEG ether at 1100 cm^{-1}.

bands do not reveal any evident intensity change up to 250 °C. Between 250 and 300 °C the signals related to the aliphatic, etheric, and esteric groups start to decrease, while the bands of the carboxylate moieties are much more evident. At 350 °C etheric, esteric, and aliphatic moieties are reduced by ∼70−80%, while the carboxylate groups are still slightly increasing. These two opposite trends continue up to 450 °C, when both vibrational bands associated with the carboxylate moieties disappear, together with all those related to the aliphatic, etheric, and esteric groups. Only one peak, located at 573 cm^{-1}, can now be detected and is generally associated with the longitudinal optical phonon vibration of ZnO nanostructured films.[31]

4. DISCUSSION

The main experimental observations can be summarized as follows:

(1) For temperatures below 150 °C, only the vaporization of the residual solvent from the polymeric matrix and the decomposition of the nitrates deriving from Zn salts are observed. These two processes are associated with a first endothermic event and a weight loss in the DSC-TGA curves. It is known that nitrates decompose in this temperature range,[18] and the occurrence of this process has been evidenced by preliminary Raman spectroscopy measurements not reported here. This decomposition/hydrolysis leads probably to the formation of Zn hydroxides, as suggested by the presence of a strong OH band at 3400 cm^{-1} in the early stage of the process; films of hydrogel not loaded with Zn ions show a weak intensity for the OH vibrational band during the entire thermal degradation process (results not shown).

(2) A first rearrangement of the polymeric matrix takes place between 150 and 200 °C. This is evidenced by an exothermic and nonoxidative process (observed also in inert atmosphere)

dx.doi.org/10.1021/jp407993q | J. Phys. Chem. C 2013, 117, 25108−25117

coupled to a small weight loss. In this temperature range, the EXAFS spectra detect little variation in the chemical environment of the Zn ions, which do not show any long-range order; μ-FTIR reveals no substantial change, but for the decrease of the OH signal, indicating further water desorption.

(3) At $T \cong 300$ °C the presence of small nuclei of ZnO is first detected by XAS. Apparently this initial nucleation takes place with a negligible thermal effect, but it is accompanied by an increase in the weight loss rate and by a further reduction in the intensity of the OH absorption band. This dehydroxylation process is probably responsible for the formation of the ZnO nuclei. μ-FTIR reveals also the beginning of the polymeric backbone degradation, evidenced by a decrease in the signals of its main functional groups and in the increase in the amount of carboxylate residues, generated by the degradation of polymeric esters.

(4) Between 350 and 400 °C the ZnO nuclei are completely formed, and an oxidative process, involving a significant weight loss and a strong exothermic thermal effect, produces the degradation of most of the organic matrix. HR-TEM and SAED analyses confirm the presence of ZnO particles embedded in an amorphous polymeric matrix. Diffraction effects in GID were observed only for $T \geq 400$ °C, probably due to the relatively low concentration, poor crystallinity, and small dimension of the ZnO particles. μ-FTIR shows a further degradation of the polymeric matrix, although carboxylate complexing moieties are still largely present. The persistence of an insulating shell of organic material around the ZnO particles is confirmed by the absence of any electrical conductivity at this stage and by the thickness observed by profilometric measurements, which has not yet reached the final value, corresponding to the sole ZnO layer. UV−vis transmittance spectra show the appearance of the typical ZnO absorption edge only for samples annealed at $T \geq 400$ °C, in accordance with PL spectra.

(5) The final step of the process, taking place between 400 and 500 °C, involves the growth of the ZnO nuclei to form well-defined nanocrystals and the completion of the polymer degradation: a process evidenced by the strongest exothermic peak at 440 °C, which is accompanied by a sharp final weight loss. The removal of all organic residues is also confirmed by the μ-FTIR spectra, by profilometric measurements, and by the disappearance of the PL band relative to the organic matrix. A sharp increase in the electrical conductivity of the film is observed for samples annealed at 450 °C, indicating the presence of a good contact between the ZnO nanoparticles. The UV−vis spectrum shows the feature of a pure ZnO sample, while the typical luminescence band is observed in the corresponding PL spectrum.

These results allow a better understanding of the mechanism responsible for the nucleation and growth of the nanoparticles resulting from the thermal degradation of the metal-loaded polymers. Taking advantage of the EXAFS ability to detect small amounts of materials, even when present in amorphous or glassy form, we have been able to produce clear evidence of ZnO nucleation even at temperature as low as 300 °C. These first nuclei are characterized by a limited level of crystallinity, but evidence of well-crystallized ZnO particles can already be observed at 350 °C. These findings are somehow in contrast with what reported by other authors using PAD techniques, which often report the formation of well crystallized metal oxide only at temperature between 450 and 500 °C, in association with the final stage of the polymer degradation.[21,22] This difference can obviously be related to the different nature of the polymers, but it can also be explained by the higher sensitivity of EXAFS in comparison with other tools such as Raman and XRD.[21,22] It must also be noted that the appearance of ZnO nuclei does not seem to be associated with any relevant thermal effect or weight loss, so it does not seem to be triggered by any specific modification of the structure of the polymer, suggesting that the nucleation is controlled only indirectly by the polymer degradation. That a temperature as low as 350 °C is enough to provide crystallization is confirmed by the fact that samples annealed at this temperature for much longer time can indeed reach full crystallization. While for $T < 350$ °C the removal of the organic matrix is incomplete also for annealing time of 24 h, for $T = 350$ °C the organic matrix is completely removed in 10 h, leading to a transparent film, which shows characteristics similar to those observed for samples annealed at 450 and 500 °C for 20 min. EXAFS and EXAFS FT analyses of these samples (Figure 14 and Table 2) confirm the presence of the NNN coordination shell with characteristics similar to those observed in samples annealed for only 20 min at 350 and 400 °C. However, the grain size was considerably reduced, to only 7 nm, which compares with the 15−20 nm observed in samples annealed at 450−500 °C for 20 min. So, the use of long annealing time at lower temperatures appears to be particularly promising for the synthesis of films characterized by extremely small grain size or for the synthesis of ZnO films on temperature-sensitive substrates.[32]

The persistence of the organic matrix encapsulating the ZnO nuclei, which is maintained during much of the thermal degradation, is probably responsible for the remarkable characteristics of the produced ZnO films because it guarantees an intimate hybridization at the nanoscale.[33] Indeed, neither precipitation nor phase separation occurs after removal of the solvent because at this stage the polymeric matrix is closely bonded to the Zn ions, as revealed by the EXAFS results. At higher temperatures a shell of carboxylates and other byproducts of the PEG degradation still encapsulates the growing particles, as evident from the TEM analysis. The encapsulation of the inorganic phase in the organic shell allows to control the ZnO grain growth and to yield high quality crack-free films over a wide range of thicknesses. The sol−gel method, on the other hand, can produce oxide films with a thickness larger than 200 nm only with great difficulty.[22] In this case the gel degradation produces a loose structure, which collapses in the last stages of the process, resulting in a high tensile stress buildup[33] and in the formation of microcracks. On the contrary, in the case of hydrogels, condensation and pore collapse are limited,[16,22] whereas structural relaxation is promoted by the soft, yielding organic phase, avoiding crack formation. This offers the possibility to prepare thick films, up to 1 μm in thickness, which are usually difficult to produce with other techniques.

5. CONCLUSIONS

The sensitivity provided by the fluo-XAFS technique allowed the inspection of the first instants of ZnO nucleation during thermal degradation of a Zn-loaded hydrogel and the determination of the temperature at which this process begins, following the evolution of the ZnO nanoparticles for increasing temperatures. By combining the results with those obtained from other techniques, such as μ-FTIR, HR-TEM, X-ray and electronic diffraction, UV−vis, impedance, and PL spectroscopies, it was possible to elucidate the nature of the close connection between the hydrogel matrix degradation and the

dx.doi.org/10.1021/jp407993q | J. Phys. Chem. C 2013, 117, 25108−25117

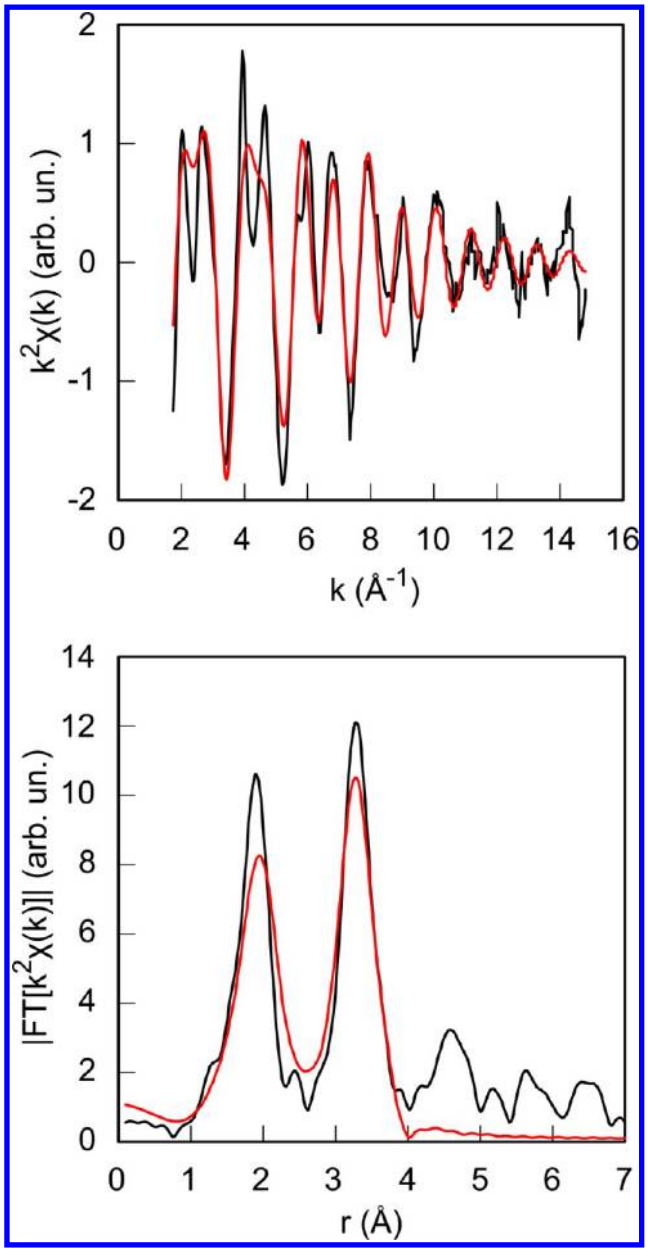

Figure 14. EXAFS spectrum (upper part) and FT (lower part) for the sample heated at 350 °C for 10 h (red line: fit; black line: experimental). For fitting results see Table 2.

Table 2. EXAFS Fitting Results for the Sample Annealed at 350 °C for 10 h

shell	N	atom	r (Å)	σ^2 (Å^2)	r_0 (Å)
1	1	O	2.03(1)	$12(2) \times 10^{-3}$	1.796
2	3	O	2.03(1)	$12(2) \times 10^{-3}$	2.042
3	6	Zn	3.23(1)	$6(2) \times 10^{-3}$	3.2089
4	6	Zn	3.36(3)	$11(4) \times 10^{-3}$	3.2490

nucleation of the ZnO nanoparticles. It has been clarified that the ZnO nanoparticles start to nucleate at 300 °C and to crystallize at 350 °C, whereas the backbone of the hydrogel starts to degrade at 300 °C, releasing carboxylate moieties and organic residuals, which constitute an insulating organic shell around the ZnO nanoparticles. At 400 °C, even though the ZnO nanoparticles are completely formed, the insulating shell is still present and its complete removal is achieved only at 450 °C. At this temperature the film has all the optical and electrical properties of a completely formed ZnO film. Prolongation of degradation time to 10 h allows to obtain the same results at 350 °C, but with smaller particle size (7 nm). The formation mechanism was clarified, suggesting a relation between the quality of the film obtained and the intimate hybridization, which takes places starting from the initial ZnO nucleation steps, until the completion of the ZnO thin film formation.

■ ASSOCIATED CONTENT

Supporting Information

Experimental details. This material is available free of charge via the Internet at http://pubs.acs.org.

■ AUTHOR INFORMATION

Corresponding Author

*E-mail tau@unipv.it, Tel +39-0382-987799 (U.A.-T.).

Notes

The authors declare no competing financial interest.

■ ACKNOWLEDGMENTS

The authors thank Dr. Irene Quinzeni (University of Pavia, Department of Chemistry) for profilometric measurements, Prof. Pietro Galinetto (University of Pavia, Department of Physics) for Raman measurements, Prof. Filippo Maglia (University of Pavia, Department of Chemistry) for intellectual support, and Laboratorio Arvedi (University of Pavia, Centro Interdipartimentale di Studi e Ricerche per la Conservazione del Patrimonio Culturale) for providing the TESCAN Mira 3 scanning electron microscope.

■ REFERENCES

(1) Özgür, Ü.; Alivov, Ya. I.; Liu, C.; Teke, A.; Reshchikov, M. A.; Doğan, S.; Avrutin, V.; Cho, S.-J.; Morkoc, H. A Comprehensive Review of ZnO Materials and Devices. *J. Appl. Phys.* **2005**, *98*, 041301−1−103.

(2) Cramer, G. Fabrication and Comparison ZnO Thin Film Transistors Various Gate Insulators, *ELECTRONICS NNIN REU 2006 Research Accomplishments*; pp 34−35.

(3) Li, C.; Li, Y.; Wu, Y.; Ong, B. S.; Loutfy, R. O. ZnO Field-Effect Transistors Prepared by Aqueous Solution-Growth ZnO Crystal Thin Film. *J. Appl. Phys.* **2007**, *102*, 076101−1−3.

(4) Prashanthi, K.; Naresh, M.; Seena, V.; Thundat, T.; Ramgopal Rao, V. A Novel Photoplastic Piezoelectric Nanocomposite for MEMS Applications. *J. Microelectromech. Syst.* **2012**, *21*, 259−261.

(5) Sudhir, C.; Atul, V. S. Preparation and Characterization of Piezoelectric Films of ZnO and AlN by RF Sputtering for RF MEMS Applications. *Key Eng. Mater.* **2012**, *500*, 84−89.

(6) Eranna, G.; Joshi, B. C.; Runthala, D. P.; Gupta, R. P. Oxide Materials for Development of Integrated Gas Sensors - A Comprehensive Review. *Crit. Rev. Solid State* **2004**, *29*, 111−188.

(7) Pandya, H. J.; Chandra, S.; Vyas, A. L. Integration of ZnO Nanostructures with MEMS for Ethanol Sensor. *Sens. Actuators, B* **2012**, *161*, 923−928.

(8) Hong, S.-K.; Hanada, T.; Ko, H.-J.; Chen, Y.; Yao, T.; Imai, D.; Araki, K.; Shinohara, M.; Saitoh, K.; Terauchi, M. Control of Crystal Polarity in a Wurtzite Crystal: ZnO Films Grown by Plasma-assisted Molecular-Beam Epitaxy on GaN. *Phys. Rev. B* **2002**, *65*, 115331−1−10.

(9) Li, X.; Yan, Y.; Gessert, T. A.; DeHart, C.; Perkins, C. L.; Young, D.; Coutts, T. J. p-type ZnO Thin Films Formed by CVD Reaction of Diethylzinc and NO Gas. *Electrochem. Solid-State Lett.* **2003**, *6*, C56−C58.

(10) Gupta, R. K.; Ghosh, K.; Patel, R.; Mishra, S. R.; Kahol, P. K. Structural, Optical and Electrical Properties of In Doped CdO Thin

Films for Optoelectronic Applications. *Mater. Lett.* **2008**, *62*, 3373−3375.
(11) Boyle, T. J.; Ward, T. L.; De'Angeli, S. M.; Xu, H.; Hammetter, F. Properties of MOCVD Deposits Using Novel Sn(II) Neo-pentoxide Precursors. *Chem. Mater.* **2003**, *15*, 765−775.
(12) Schwartz, R. W.; Schneller, T.; Waser, R. Chemical Solution Deposition of Electronic Oxide Films. *C. R. Chim.* **2004**, *7*, 433−461.
(13) Parikh, H.; De Guire, M. R. Recent Progress in the Synthesis of Oxide Films from Liquid Solutions. *J. Ceram. Soc. Jpn.* **2009**, *117*, 228−235.
(14) Tredici, I. G.; Yaghmaie, F.; Irving, M.; Wijesundara, M. B. J.; Maglia, F.; Quartarone, E.; Galinetto, P.; Anselmi-Tamburini, U. Micropatterned Nanocrystalline Zinc Oxide Thin Films Obtained Through Metal-loaded Hydrogels. *Thin Solid Films* **2011**, *519*, 5854−5860.
(15) Tredici, I. G.; Yaghmaie, F.; Irving, M.; Wijesundara, M. B. J.; Maglia, F.; Quartarone, E.; Anselmi-Tamburini, U. Solution Deposition of Micropatterned Nanocrystalline Metal Oxide Films Through Hydrogels. *J. Am. Ceram. Soc.* **2011**, *94*, 3171−3174.
(16) Tredici, I. G.; Maglia, F.; Resmini, A.; Anselmi-Tamburini, U. Solution Deposition of Micropatterned TiO_2, ZrO_2, SnO_2, and In_2O_3 Thin Films Through Metal-loaded Hydrogels. *Thin Solid Films* **2013**, *542*, 52−59.
(17) Tredici, I. G.; Resmini, A.; Yaghmaie, F.; Irving, M.; Maglia, F.; Anselmi-Tamburini, U. A Simple Two-Step Solution Chemistry Method for Synthesis of Micropatterned ZnO Nanorods Based on Metal-Loaded Hydrogels. *Thin Solid Films* **2012**, *526*, 22−27.
(18) Kim, G. H.; Shin, H. S.; Ahn, B. D.; Kim, K. H.; Park, W. J.; Kim, H. J. Formation Mechanism of Solution-Processed Nanocrystalline InGaZnO Thin Film as Active Channel Layer in Thin-Film Transistor. *J. Electrochem. Soc.* **2009**, *156*, H7−H9.
(19) Ong, B. S.; Li, C.; Li, Y.; Wu, Y.; Loutfy, R. Stable, Solution-Processed, High-Mobility ZnO Thin-Film Transistors. *J. Am. Chem. Soc.* **2007**, *129*, 2750−2751.
(20) Lee, D.-H.; Chang, Y.-J.; Herman, G. S.; Chang, C.-H. A General Route to Printable High-Mobility Transparent Amorphous Oxide Semiconductors. *Adv. Mater.* **2007**, *19*, 843−847.
(21) Kang, L.; Gao, Y.; Luo, H. A Novel Solution Process for the Synthesis of VO_2 Thin Films with Excellent Thermochromic Properties. *ACS Appl. Mater. Interfaces* **2009**, *1*, 2211−2218.
(22) Jia, Q. X.; McCleskey, T. M.; Burrell, A. K.; Lin, Y.; Collis, G. E.; Wang, H.; Li, A. D. Q.; Foltyn, S. R. Polymer-Assisted Deposition of Metal-Oxide Films. *Nat. Mater.* **2004**, *3*, 529−532.
(23) Ghigna, P.; Pin, S.; Spinolo, G.; Newton, M. A.; Zema, M.; Tarantino, S. C.; Capitani, G.; Tatti, F. μ-XANES Mapping of Buried Interfaces: Pushing Microbeam Techniques to the Nanoscale. *Phys. Chem. Chem. Phys.* **2010**, *12*, 5547−5550.
(24) Pin, S.; Newton, M. A.; D'Acapito, F.; Zema, M.; Tarantino, S. C.; Spinolo, G.; De Souza, R. A.; Martin, M.; Ghigna, P. Mechanisms of Reactions in the Solid State: (110) Al_2O_3 + (001) ZnO Interfacial Reaction. *J. Phys. Chem. C* **2012**, *116*, 980−986.
(25) Pin, S.; Ghigna, P.; Spinolo, G.; Quartarone, E.; Mustarelli, P.; D'Acapito, F.; Migliori, A.; Calestani, G. Nanoscale Formation of New Solid-State Compounds by Topochemical Effects: the Interfacial Reactions ZnO with Al_2O_3 as a Model System. *J. Solid State Chem.* **2009**, *182*, 1291−1296.
(26) Bellitto, C.; Gastaldi, L.; Tomlinson, A. A. G. Crystal Structure of Tetraphenyiarsonium Tetranitratozincate(2−), and Optical Spectrum of Tetranitratocobaltate(2−). *J. Chem. Soc., Dalton Trans.* **1976**, 989−992.
(27) Viswanatha, R.; Sapra, S.; Satpati, B.; Satyam, P. V.; Dev, B. N.; Sarma, D. D. Understanding the Quantum Size Effects in ZnO Nanocrystals. *J. Mater. Chem.* **2004**, *14*, 661−668.
(28) Collins, R. J.; Thomas, D. G. Photoconduction and Surface Effects with Zinc Oxide Crystals. *Phys. Rev.* **1958**, *112*, 388−395.
(29) Znaidi, L.; Soler Illia, G. J. A. A.; Le Guennic, R.; Sanchez, C.; Kanaev, A. Elaboration of ZnO Thin Films with Preferential Orientation by a Soft Chemistry Route. *J. Sol-Gel Sci. Technol.* **2003**, *26*, 817−821.
(30) Anzlovar, A.; Orel, Z. C.; Zigon, M. Poly(methyl methacrylate) Composites Prepared by In Situ Polymerization Using Organophillic Nano-to-Submicrometer Zinc Oxide Particles. *Eur. Polym. J.* **2010**, *46*, 1216−1224.
(31) Jana, S.; Vuk, A. S.; Mallick, A.; Orel, B.; Biswas, P. K. Effect of Boron Doping on Optical Properties of Sol−Gel Based Nanostructured Zinc Oxide Films on Glass. *Mater. Res. Bull.* **2011**, *46*, 2392−2397.
(32) Kim, Y.-H.; Heo, J.-S.; Kim, T.-H.; Park, S.; Yoon, M.-H.; Kim, J.; Oh, M. S.; Yi, G.-R.; Noh, Y.-Y.; Park, S. K. Flexible Metal-Oxide Devices Made by Room-Temperature Photochemical Activation of Sol-Gel Films. *Nature* **2012**, *489*, 128−132.
(33) Kozuka, H.; Kajimura, M. Single-Step Dip Coating of Crack-Free $BaTiO_3$ Films >1 μm Thick: Effect of Poly(vinylpyrrolidone) on Critical Thickness. *J. Am. Ceram. Soc.* **2000**, *83*, 1056−1062.